The Structure of a Novel Insect Peptide Explains Its Ca^{2+} Channel Blocking and Antifungal Activities[†,‡]

Takahide Kouno,[§] Mineyuki Mizuguchi,*[,§] Hiromasa Tanaka,[||] Ping Yang,[||] Yoshihiro Mori,[§] Hiroyuki Shinoda,[§] Kana Unoki,[§] Tomoyasu Aizawa,[⊥] Makoto Demura,[⊥] Koichi Suzuki,[||] and Keiichi Kawano[⊥]

Faculty of Pharmaceutical Sciences, University of Toyama, Toyama 930-0194, Faculty of Agriculture, Iwate University, Morioka 020-8550, and Division of Biological Sciences, Graduate School of Science, Hokkaido University, Sapporo 060-0810, Japan

Received July 5, 2007; Revised Manuscript Received September 19, 2007

ABSTRACT: Diapause-specific peptide (DSP), derived from the leaf beetle, inhibits Ca^{2+} channels and has antifungal activity. DSP acts on chromaffin cells of the adrenal medulla in a fashion similar to that of ω-conotoxin GVIA, a well-known neurotoxic peptide, and blocks N-type voltage-dependent Ca^{2+} channels. However, the amino acid sequence of DSP has little homology with any other known Ca^{2+} channel blockers or antifungal peptides. In this paper, we analyzed the solution structure of DSP by using two-dimensional ^{1}H nuclear magnetic resonance and determined the pairing of half-cystine residues forming disulfide bonds. The arrangement of the three disulfide bridges in DSP was distinct from that of other antifungal peptides and conotoxins. The overall structure of DSP is compact due in part to the three disulfide bridges and, interestingly, is very similar to those of the insect- and plant-derived antifungal peptides. On the other hand, the disulfide arrangement and the three-dimensional structure of DSP and GVIA are not similar. Nevertheless, some surface residues of DSP superimpose on the key functional residues of GVIA. This homologous distribution of hydrophobic and charged side chains may result in the functional similarity between DSP and GVIA. Thus, we propose here that the three-dimensional structure of DSP can explain its dual function as a Ca^{2+} channel blocker and antifungal peptide.

Diapause-specific peptide (DSP),[1] which was isolated from the leaf beetle *Gastrophysa atrocyanea*, is a 41-residue peptide with 6 cysteine residues (Figure 1) (*1*). DSP is expressed in the hemolymph and fat bodies of the insect. This insect lives in the soil at two periods in its life, from pupa to adult and during diapause of the mature insect. Interestingly, DSP appears only during the latter period (*1*, *2*), suggesting that it plays a role in diapause of the adult leaf beetle. An RNA interference study, however, found that inhibition of DSP expression does not affect the onset or maintenance of diapause. Taken together, these findings indicate that the expression of DSP accompanies but does not play a direct role in the induction or maintenance of diapause.

In addition to the interesting expression pattern, DSP has some unique properties, namely, inhibition of the voltage-dependent Ca^{2+} channel and antifungal activity (*3*). DSP dose-dependently blocks Ca^{2+} influx into bovine adrenal chromaffin cells without affecting catecholamine secretion. Considering that ω-conotoxin GVIA, an N-type Ca^{2+} channel blocker derived from the venom of the fish-hunting cone shell *Conus geographus*, acts in a similar fashion (*4*), DSP most likely targets the N-type Ca^{2+} channel ($Ca_V2.2$). However, there is no sequence homology between DSP and GVIA except for the presence of six cysteine residues (*3*). The cysteine residues in GVIA form three disulfide bonds, conferring a compact and rigid conformation referred to as the inhibitory cystine knot (ICK) motif (*5*−*7*). The ICK motif includes a triple-stranded, antiparallel β-sheet stabilized by a cystine knot that consists of a characteristic arrangement of disulfide bridges, wherein two bridges and the interconnecting backbone form a ring through which the third bridge passes. This motif is common in the ion channel-targeting toxins of spiders and cone shells, for example, ω-agatoxin IVB (P-type Ca^{2+} channel blocker) (*8*, *9*), ω-conotoxin GVIA (N-type Ca^{2+} channel blocker) (*10*, *11*), and conotoxin GS (Na^+ channel blocker) (*12*, *13*). Peptides with the ICK motif have the consensus sequence $CX_{3-7}CX_{3-6}CX_{0-5}CX_{1-4}CX_{4-13}C$, where C represents a half-cystine and X represents any other

[†] This study was supported by grants from the Ministry of Education, Culture, Sports, Science and Technology of Japan (MEXT), a Grant-in-Aid from the 21st Century Center of Excellence Program (COE) (MEXT), the National Project on Protein Structural and Functional Analyses (MEXT), and the Research and Development Program for New Bio-industry Initiatives (BRAIN).

[‡] The ^{1}H chemical shifts and the atomic coordinates of DSP with disulfide bonds Cys-7/Cys-21, Cys-11/Cys-33, and Cys-22/Cys40 were deposited in the BioMagResBank as entry 6729 and the Protein Data Bank as entry 2E2F, respectively.

* To whom correspondence should be addressed. Phone: 81-76-434-7595. Fax: 81-76-434-5061. E-mail: mineyuki@pha.u-toyama.ac.jp.

[§] University of Toyama.

[||] Iwate University.

[⊥] Hokkaido University.

[1] Abbreviations: CS$\alpha\beta$, cysteine-stabilized α-helix and β-sheet; DQF-COSY, double-quantum-filtered correlation spectroscopy; DSP, diapause-specific peptide; GVIA, ω-conotoxin GVIA; ICK, inhibitory cystine knot; MVIIA, ω-conotoxin MVIIA; NMR, nuclear Overhauser enhancement; NOESY, NOE spectroscopy; PhD1, *Petunia hybrida* defensin 1; rms, root mean square; Rs-AFP, *Raphanus sativus*-antifungal peptide; TOCSY, total correlation spectroscopy.

10.1021/bi701319t CCC: $37.00
Published on Web 11/10/2007

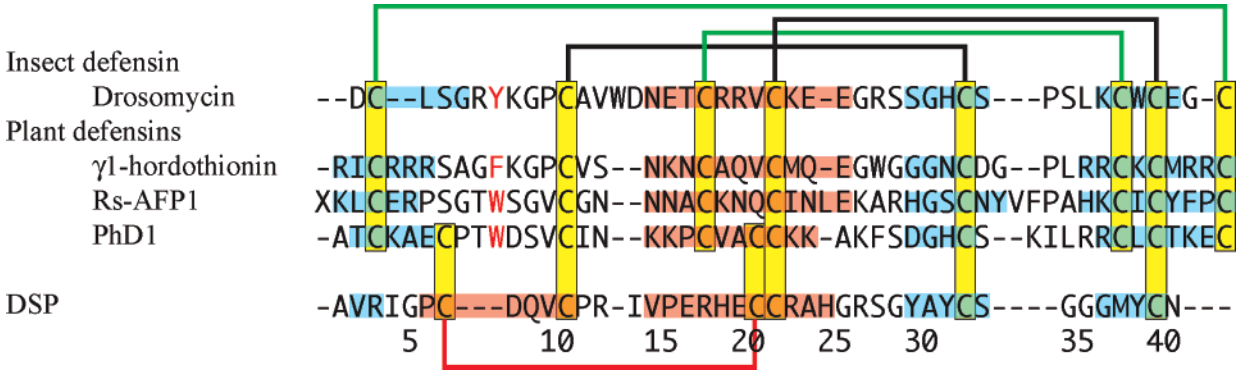

FIGURE 1: Sequence alignment of DSP and other peptides. Amino acid residues are numbered according to the DSP sequence. X is the one-letter code for pyroglutamic acid. The half-cystine residues are highlighted by yellow boxes, and the disulfide bonds are depicted by connecting lines. Peptides in the PDB with structural similarity to DSP were found using DALI (*41*) and PAPIA (*42*). The sequences were aligned with CLUSTAL-W. The structural data were obtained from the PDB (drosomycin, PDB code 1MYN (*19*); γ1-hordothionin, 1GPT (*44*); Rs-AFP1, 1AYJ (*20*); PhD1, 1N4N (*43*)). Residues included in α-helices and β-strands are indicated by red and blue shading, respectively. The disulfide bonds shown by green lines are not found in DSP, whereas the disulfide bond indicated with a red line is found only in DSP and PhD1. The aromatic residues conserved in drosomycin, γ1-hordothionin, Rs-AFP1, and PhD1 are highlighted in red.

amino acid (*5*−*7*). The diversity of their functions and specificities is due to differences in the gaps between the half-cystine residues. Nielsen et al. (*14*) examined the activities of hybrid peptides generated from ω-conotoxins MVIIA and MVIIC, which have a common sequence, $CX_6CX_6CCX_3CX_{4-5}C$, and are selective for N- and P/Q-type Ca^{2+} channels, respectively. They found that the second and the fourth gaps play an important role in control of the selectivity for these two Ca^{2+} channels, whereas the first and the third gaps have little influence on the selectivity. On the other hand, site-directed mutation studies to identify the residues essential for the interaction of GVIA with the Ca^{2+} channel have revealed that Tyr-13 is the most important for the channel blocking activity (*15*−*17*). This residue is located at a position corresponding to the second gap in the MVIIA and MVIIC sequences.

Insects and plants have several families of antifungal peptides. These have the characteristic disulfide bridge pattern but lack the ICK motif. One of these families has a double-stranded, antiparallel β-sheet and an additional α-helix structure, which together are referred to as the cysteine-stabilized α-helix and β-sheet (CSαβ) motif (*18*). For example, drosomycin (from *Drosophila melanogaster*) and *Raphanus sativus*-antifungal peptide (Rs-AFP) contain a CSαβ motif (*19*, *20*) and have antifungal activity (*21*, *22*). Although two of three disulfide bridges in the CSαβ motif and the interconnecting backbone form a ring, the remaining bridge does not pass through the ring unlike the ICK motif. In addition, the amino acid sequence in the CSαβ motif does not satisfy the consensus sequence of the ICK motif (*5*, *7*). Consistent with these differences, Rs-AFP does not block Ca^{2+} channels (*23*) but rather stimulates rapid Ca^{2+} uptake by fungal hyphae (*24*, *25*). Rs-AFP also induces membrane permeabilization and inhibits fungal growth. Recently, the target of Rs-AFP was found to be a specific glucosylceramide, a membrane component of fungi (*26*). This may be involved in the membrane permeabilization and subsequent arrest of fungal growth, although the detailed mechanism of fungal growth inhibition remains to be elucidated.

The amino acid sequence of DSP can be represented as $CX_3CX_9CCX_{10}CX_6C$, wherein the six cysteine residues form three disulfide bonds (*3*). The second and third gaps are too long to satisfy a consensus sequence for an ICK motif. Although the peptide mapping using DSP identified one of three disulfide bridges, specifically, between the second (Cys-11) and the fifth (Cys-33) half-cystine residues, the arrangement of the remaining disulfide bridges has not been clear. Here, we analyzed the solution structure of intact DSP derived from diapausing adult leaf beetles and elucidated the half-cystine pairings. Interestingly, our nuclear magnetic resonance (NMR) data suggested that the disulfide bridge pattern of DSP is different from those of ω-conotoxins and other antifungal peptides. Nevertheless, DSP adopts a compact overall structure similar to those of drosomycin and Rs-AFP and contains a CSαβ-like structure. Moreover, DSP and ω-conotoxin have similar arrangements of surface residues, even though the overall folds are different. These residues of GVIA have been found to play a role in the interaction with its target, the Ca^{2+} channel. Thus, the structural similarity can explain the dual function of DSP as a Ca^{2+} channel blocker and antifungal peptide.

EXPERIMENTAL PROCEDURES

Preparation of Intact DSP. The intact DSP was isolated and purified from the diapausing adults of the leaf beetle (*G. atrocyanea*) (*1*, *3*). The purified DSP was lyophilized and cryopreserved until further analysis. The purity and the integrity of DSP were confirmed by mass spectrometry.

NMR Spectroscopy. Lyophilized DSP was dissolved in 250 μL of aqueous buffer (10 mM sodium phosphate, pH 7.0, 50 mM NaCl, and 5% or 100% D_2O) and centrifuged at 15000*g* for 1 min to remove aggregated protein. The protein concentration of the supernatant was estimated to be 0.15 mM according to the absorbance at 280 nm and the molar extinction coefficient based on the numbers of tyrosine and half-cystine residues in DSP ($\epsilon = 4845\ M^{-1}\ cm^{-1}$) (*27*). All of the NMR spectra were acquired at 298 K on a Bruker AV800 spectrometer equipped with a cryogenic probe. DQF-COSY (*28*), TOCSY (mixing time 50 and 75 ms) (*29*), and NOESY (50, 100, and 150 ms) (*30*) spectra were acquired with solvent suppression using the WATERGATE sequence (*31*). DQF-COSY was recorded with 4096 × 512 data points, and the other spectra were recorded with 2048 × 512 data points and 96 scans. ^1H chemical shifts were directly referenced to the resonance of 2,2-dimethyl-2-silapentane-

5-sulfonate sodium salt. The assignments of ^{1}H resonances of the backbone and the side chains were performed using a series of two-dimensional NMR experiments as described previously (*32*). The $^3J_{HNH\alpha}$ coupling constants derived from the DQF-COSY spectrum were used for estimation of dihedral angles (ϕ) according to the Karplus equation. Furthermore, 2 h after DSP was dissolved in 100% D_2O buffer, slowly exchanging amide protons were identified from the TOCSY spectrum. All NMR spectra were processed and analyzed using NMRPipe (*33*), PIPP (*34*), and NMRView (*35*) software.

Structure Calculations. For structure calculations of DSP, distance restraints were collected from two-dimensional homonuclear NOESY spectra acquired with a 100 ms mixing time in 5% or 100% D_2O buffer. The initial assignment of NOE cross-peaks was performed using a manual procedure. This process assigned the cross-peaks without overlapping or ambiguous assignments. To progress the NOE assignment, an automated assignment protocol was carried out using the "noeassign" script supplied with CYANA (*36*, *37*). The peak lists derived from the manual assignments were used for the NOE assignment and the structure calculations with CYANA. In this process, the disulfide bond between Cys-11 and Cys-33 was applied as the distance restraint; specifically, the restraints for the $CysS^{\gamma}-CysS^{\gamma}$ and $CysS^{\gamma}-CysC^{\beta}$ distances were assigned to be 2.00−2.10 and 3.00−3.10 Å, respectively. The final NOE restraints obtained from CYANA were used to calculate a family of 50 structures in X-PLOR using simulated annealing protocols (*38*). In addition to the NOE distance restraints, the disulfide bond between Cys-11 and Cys-33, the dihedral angle, and the hydrogen bond information were used. The hydrogen bonds were identified according to amide protons that exchanged slowly with the solvent deuterium, and their partners were assigned on the basis of the structure calculations with CYANA. For hydrogen bonds, distance restraints of 2.30−3.30 and 1.30−2.30 Å were used for N−O and HN−O atom pairs, respectively. A simulated annealing protocol was applied using 12 000 steps at high temperature (1000 K) and 8000 steps for the cooling process. A total of 50 structures were calculated, and the 25 lowest energy structures were used for calculation of the energy-minimized average structure.

To resolve the half-cystine parings of the two disulfide bonds consisting of Cys-7, Cys-21, Cys-22, and Cys-40, further calculations were performed on the basis of the structure derived from the previous calculations. Three pairing patterns of the disulfide bonds were feasible: (i) Cys-7/Cys-21 and Cys-22/Cys-40, (ii) Cys-7/Cys-22 and Cys-21/Cys-40, and (iii) Cys-7/Cys-40 and Cys-21/Cys-22. In each case, X-PLOR calculations were performed using the distance restraints describing the respective disulfide bonds. Finally, the structures with each disulfide pattern were compared, and the pattern giving the lowest energy was adopted as a correct disulfide arrangement. The obtained structures were analyzed with MOLMOL (*39*) and PROCHECK-NMR (*40*) software. Structural figures were generated using the MOLMOL program.

Gel Filtration Chromatography. To estimate the apparent molecular weight of DSP, gel filtration chromatography was performed using a Superdex 75 HR 10/30 column (Amersham Biosciences/GE Healthcare). The column was equilibrated with running buffer (10 mM sodium phosphate, pH 7.0, and 150 mM NaCl) at 4 °C. After NMR experiments, 25 μL of DSP solution was applied to the column, and the column was eluted at a flow rate of 0.4 mL/min. Ribonuclease A (13.7 kDa), aprotinin (6.5 kDa), and vitamin B_{12} (1.4 kDa) were used as molecular mass standards. All eluted components were detected by absorbance at 280 nm.

RESULTS

NMR Analysis of DSP. We successfully obtained the NMR spectra to analyze and calculate the solution structure of DSP. Sequence-specific assignment for almost all backbone amide protons in DSP (except for Ala-1, Gly-35, and Gly-36) was achieved using the two-dimensional TOCSY and NOESY spectra (Figure S1 in the Supporting Information). A survey of the sequential and medium-range NOE assignments (Figure S2A in the Supporting Information) was used for the identification of the secondary structure elements. The NOE cross-peaks of $d_{\alpha N}(i, i + 3)$ and $d_{\alpha\beta}(i, i + 3)$ indicated that the two regions (residues 5−13 and 15−25) of DSP form a helical conformation and that the remainder has little recognizable secondary structure. Some of the characteristic NOE connectivities shown in Figure S2B, however, suggested that DSP includes an antiparallel β-sheet structure formed by three short strands. Three resonances derived from amide protons (Val-2, Tyr-32, and Tyr-39) were significantly detected in the TOCSY spectrum recorded 2 h after the lyophilized DSP was dissolved in 100% D_2O buffer, implying that they participate in hydrogen bond formation. This observation agrees with a β-sheet structure as suggested by the NOE connectivities (Figure S2B).

As a result of the automated NOE assignment with CYANA, a total of 408 NOE-derived distance restraints were collected for the structure calculation (195 intraresidual, 95 sequential, 56 medium-range, and 62 long-range restraints). The DSP structure calculated with CYANA supported the idea that the amide protons of Val-2, Tyr-32, and Tyr-39 form hydrogen bonds with the carbonyl oxygens of Cys-40, Tyr-39, and Tyr-32, respectively. The following X-PLOR calculations incorporated these three hydrogen bonds as well as a disulfide bond between Cys-11 and Cys-33 as distance restraints. A total of 417 distance and 24 ϕ angle restraints were used for the X-PLOR calculations, yielding a well-defined structure with a backbone root-mean-square (rms) deviation value of 0.46 ± 0.10 Å for assigned residues 2−34 and 37−41 (Table 1). Although the calculation used information for only one disulfide bond, Cys-11/Cys-33, the global fold of DSP was very compact. The remaining half-cystines, Cys-7, Cys-21, Cys-22, and Cys-40, are in close proximity even in the DSP structure that was obtained from the calculation without the disulfide bond information. This may be due to the presence of NOE restraints between these half-cystine residues such as Cys-7 H^{β}/Cys-21 H^{β} and Cys-22 H^{β}/Cys-40 H^{β} (Figure S1B), which is consistent with the fact that these residues form disulfide bridges.

Determination of the Disulfide Bridge Pattern of DSP. To resolve the disulfide arrangement of DSP, three possible disulfide patterns were considered, and calculations were carried out for each to evaluate to what extent they agreed with the experimental data. The respective disulfide and hydrogen bond information was incorporated into the X-PLOR calculation, generating three structure ensembles with

Table 1: Structural Statistics for the 25 Calculated Structures of DSP with Different Disulfide Bond Patterns

	Cys-11/Cys-33	i[a]	ii[b]	iii[c]
X-PLOR energies (kJ mol^{-1})				
E_{total}	71.71 ± 1.52	73.74 ± 1.73	244.47 ± 22.64	169.60 ± 4.33
E_{bonds}	2.26 ± 0.12	2.23 ± 0.14	17.00 ± 1.73	16.88 ± 0.86
E_{angles}	50.52 ± 0.61	51.74 ± 0.77	106.87 ± 5.84	84.91 ± 3.17
$E_{improper}$	8.80 ± 0.34	9.22 ± 0.26	22.21 ± 2.85	27.55 ± 1.04
$E_{van\ der\ Waals}$	3.55 ± 0.34	3.81 ± 0.38	41.40 ± 12.74	26.53 ± 3.46
E_{NOE}	5.88 ± 0.96	5.84 ± 0.62	50.99 ± 7.90	12.02 ± 1.44
$E_{dihedral}$	0.69 ± 0.13	0.90 ± 0.22	6.01 ± 0.98	1.72 ± 0.73
rms deviations from idealized covalent geometry				
bonds (Å)	0.001935 ± 0.000010	0.001922 ± 0.000062	0.005307 ± 0.000268	0.005293 ± 0.000138
angles (deg)	0.5552 ± 0.0033	0.5619 ± 0.0042	0.8072 ± 0.0222	0.7197 ± 0.0132
improper (deg)	0.4203 ± 0.0081	0.4303 ± 0.0062	0.6664 ± 0.0428	0.7436 ± 0.0141
Ramachandran plot (%)				
most favored	71.9	71.8	72.5	75.4
additional allowed	27.6	27.7	21.5	22.5
generously allowed	0.5	0.5	6.0	2.0
disallowed region	0.0	0.0	0.0	0.1
rms deviations (Å)				
all assigned residues 2−34 and 37−41				
backbone heavy atoms	0.46 ± 0.10	0.48 ± 0.11	0.65 ± 0.18	0.50 ± 0.16
all heavy atoms	1.16 ± 0.15	1.16 ± 0.14	1.33 ± 0.18	1.24 ± 0.19

[a] Cys-7/Cys-21, Cys-11/Cys-33, and Cys-22/Cys-40. [b] Cys-7/Cys-22, Cys-11/Cys-33, and Cys-21/Cys-40. [c] Cys-7/Cys-40, Cys-11/Cys-33, and Cys-21/Cys-22.

different disulfide arrangements. This survey indicated that the structure ensemble with the disulfide bridges Cys-7/Cys-21, Cys-11/Cys-33, and Cys-22/Cys-40 has the lowest energy and the minimal deviation from the idealized geometry (Table 1). The other two ensembles did not effectively satisfy the experimental restraints and had significantly large violations from the idealized geometry. The statistical values for the structure ensemble with disulfide bonds Cys-7/Cys-21, Cys-11/Cys-33, and Cys-22/Cys-40 were comparable to those for the ensemble with only one disulfide bond, Cys-11/Cys-33, indicating that incorporation of the information describing disulfide bonds Cys-7/Cys-21 and Cys-22/Cys-40 had little effect on the energy and deviation terms (Table 1).

The 25-structure ensemble with disulfide bridges Cys-7/Cys-21, Cys-11/Cys-33, and Cys-22/Cys-40 has a well-defined backbone rms deviation value of 0.48 ± 0.11 Å (Figure 2A, Table 1). According to the Ramachandran plot, all residues (except for glycine and proline) of the 25 structures with the lowest energy were within the allowable regions, and the majority (99.5%) of these were included in the most-favored and additional allowed regions. The resulting energy-minimized average structure with the three disulfide bridges is presented in Figure 2B. The backbone heavy atoms of this structure could be superimposed on those of the structure including only disulfide bridge Cys-11/Cys-33 with an rms deviation value of 0.29 Å. The agreement of the backbone trace also indicates that the additional disulfide bond information has essentially no influence on not only the X-PLOR energy terms but also the overall structure of DSP. Taken together, our NMR analysis allows us to conclude that the most likely disulfide arrangement of DSP is Cys-7/Cys-21, Cys-11/Cys-33, and Cys-22/Cys-40.

Solution Structure of DSP. The DSP structure includes two α-helices (residues 5−9 and 15−25, referred to as α1 and α2, respectively) and a triple-stranded β-sheet (residues 2−4, 30−33, and 38−40, referred to as β1, β2, and β3, respectively) (Figure 2B). The global fold is represented as β1−α1−α2−β2−β3, where β1/β3 and β2/β3 are arranged in an antiparallel fashion. The three disulfide bridges, Cys-7/Cys-21, Cys-11/Cys-33, and Cys-22/Cys-40, link α1 and α2, the α1/α2 loop and β2, and α2 and β3, respectively. Almost all secondary structures included in DSP are fixed to each other through the disulfide bonds, and as a result, the DSP structure adopts a very compact and well-defined conformation in solution. Thus, the disulfide bonds contribute to the formation of the overall DSP structure. In addition, the conformation assisted by the disulfide links seems to be involved in the surface exposure of the hydrophobic side chains of DSP. Two tyrosine residues, Tyr-32 and Tyr-39, are located in strands β2 and β3, respectively. The gel filtration results (see "Gel Filtration Chromatography" below) indicate that DSP exists as a monomer in solution. These findings indicate that the side chains of these tyrosine residues are exposed to the solvent. In aqueous solution, hydrophobic side chains are generally buried in the protein interior. In the case of DSP, the β-strands including Tyr-32 and Tyr-39 are fixed by the disulfide bridges Cys-11/Cys-33 and Cys-22/Cys-40, respectively. The conformation of DSP may therefore result in the exposure of the hydrophobic side chains of Tyr-32 and Tyr-39. Moreover, the side chain of the third tyrosine residue, Tyr-30, is also accessible to solvent; indeed, all three tyrosine residues of DSP are located on the peptide surface (Figure 2B).

Gel Filtration Chromatography. Under conditions similar to those used in the NMR experiment, DSP eluted as a single peak from the gel filtration column between the relative positions for aprotinin (6.5 kDa) and vitamin B_{12} (1.4 kDa) (Figure S3 in the Supporting Information). This analysis indicated a molecular weight of approximately 2.5 kDa, whereas the calculated molecular weight of DSP is 4.5 kDa. This inconsistency may be due to DSP having a compact globular structure. At a minimum, the gel filtration chromatography findings suggest that DSP is a monomer in solution.

DISCUSSION

Structure Calculation of DSP. In the current study, we determined the three-dimensional structure and the half-

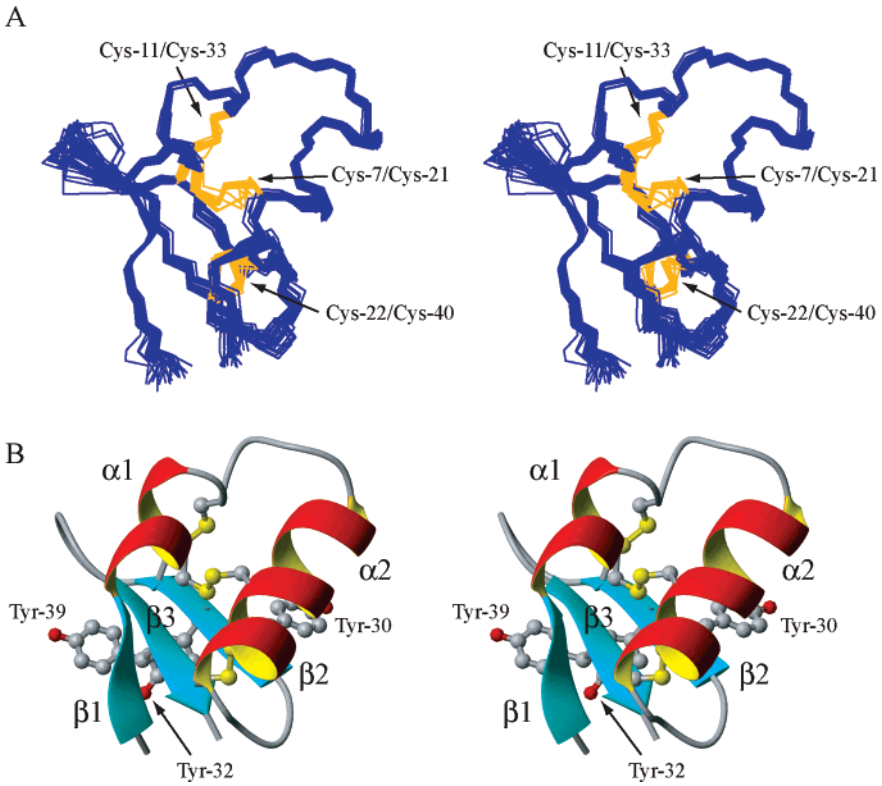

FIGURE 2: Stereoviews of the solution structure of DSP with disulfide bonds Cys-7/Cys-21, Cys-11/Cys-33, and Cys-22/Cys-40. (A) The backbone traces of the 25 lowest energy structures are superimposed using the backbone atoms (N, C^{α}, and C) for assigned residues 2−34 and 37−41. The side chain of the half-cystine residues and the disulfide bonds are shown with orange lines. (B) Ribbon representation of the energy-minimized average structure of DSP. The side chains of the half-cystine and all three tyrosine residues (Tyr-30, Tyr-32, and Tyr-39) accessible to solvent are shown with a ball-and-stick scheme. The figure was prepared using MOLMOL (*39*).

cystine pairings of DSP using NMR-based structure calculations. We used approximately 11 NOE-derived distance restraints per residue, which seems to be insufficient to determine disulfide bridge pairings. However, half of the total restraints (197 restraints), and three-quarters of the long-range restraints (47 restraints), were derived from 12 residues that contribute to a structural core of DSP, namely, Val-2, Ile-4, Cys-7, Val-10, Arg-18, Cys-21, Cys-22, Arg-27, Gly-29, Tyr-30, Met-38, and Cys-40. Residues Cys-7, Cys-21, Cys-22, and Cys-40, a major focus of this study, also participate in the core and have little solvent accessibility in the calculated structure. Because all four half-cystine residues are surrounded by other residues, structure calculation with information describing incorrect disulfide bridges would cause not only an increase in restraint violations but also van der Waals clashes. In agreement with this, structures with disulfide bond patterns ii and iii show high potential energies and large violations compared with those with pattern i (Table 1). In particular, the van der Waals ($E_{\text{van der Waals}}$) and the NOE terms (E_{NOE}) of pattern ii were about 10-fold higher than those of pattern i. Thus, the structure calculations with the NOE-derived distance restraints obtained from the automated assignment enabled identification of the most likely disulfide pairings, namely, Cys-7/Cys-21 and Cys-22/Cys-40.

Comparison of Structures of DSP and Antifungal Peptides. Using DALI (*41*) and PAPIA (*42*), we searched the Protein Data Bank (PDB) for peptides with structural similarities. We found some antimicrobial and antifungal peptides such as drosomycin (PDB code 1MYN) (*19*) and *Petunia hybrida* defensin 1 (PhD1; PDB code 1N4N) (*43*). Although these apparently share the overall structure shown in Figure 3, there are some differences in their structures. First, the secondary structure element of DSP is different from that of other antifungal peptides. Specifically, DSP possesses an α1 helix followed by a β1 strand, whereas the corresponding region in drosomycin and PhD1 does not form any secondary structure (Figure 3). In drosomycin and PhD1, the β1/α1 loop region includes a conserved aromatic residue, namely, Tyr-7 in drosomycin and Trp-10 in PhD1 (Figure 1). This aromatic side chain is directed toward their α1 helices (corresponding to α2 in DSP), which contributes to the structural convergence and the stabilization of the β1/α1 loop region due to hydrophobic interactions (*19*, *43*). Unlike the other antifungal peptides with a CSαβ fold, however, the corresponding region of DSP lacks aromatic residues and forms an α-helix structure.

Drosomycin and PhD1 include a CSαβ motif assisted by three disulfide bridges. A pair of half-cystine residues (Cys-20 and Cys-24 in PhD1) separated by three amino acids (CXXXC) in α1 are connected via disulfide bridges to a second pair of half-cystine residues (Cys-41 and Cys-43 in PhD1) located on the same strand (β3) and separated by one amino acid (CXC) (Figure 3B). The third disulfide bond is found between the β1/α1 loop and the β2 strand (Cys-14/Cys-34 in PhD1). In addition to the CSαβ motif, a fourth disulfide bridge (Cys-3/Cys-47 in PhD1) is also conserved among a variety of defensins (Figure 1). Moreover, PhD1 possesses a unique disulfide bridge connecting the β1/α1 loop with the α1 helix (Cys-7/Cys-23). DSP seems to lack two disulfide bridges found in PhD1 (Cys-3/Cys-47 and Cys-20/Cys-41) (Figure 3). Because Cys-20/Cys-41 in PhD1 is

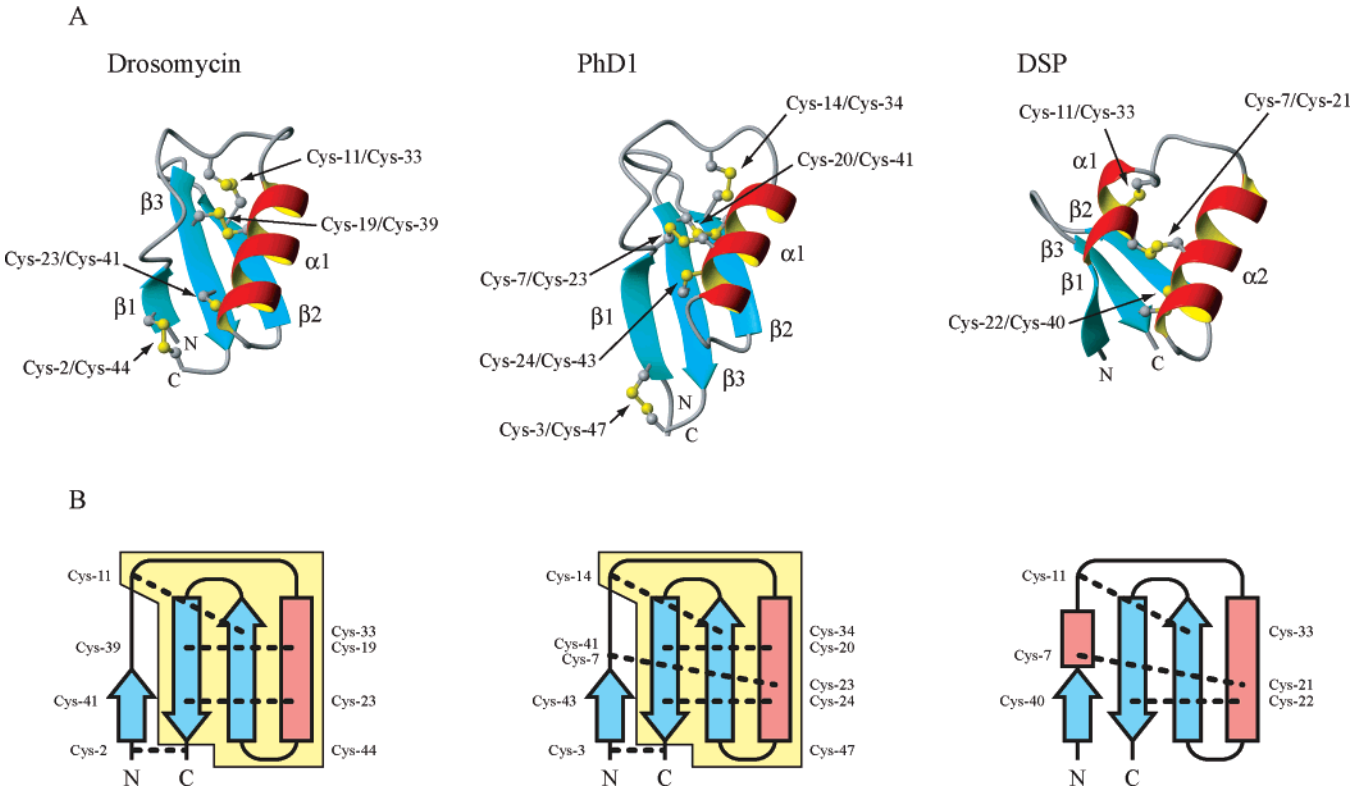

FIGURE 3: Comparison of the three-dimensional structures and the secondary structure elements among drosomycin (PDB code 1MYN, left), PhD1 (1N4N, middle), and DSP (right). (A) Ribbon representation of the solution structures. The disulfide bridges are shown with a ball-and-stick scheme. (B) Schematic diagram of the secondary structure elements. The α-helix and the *β*-strand are indicated with a cylinder and an arrow, respectively. The disulfide bridges are shown with broken lines and consist of the two-half-cystine residues labeled on both side of the panels. The yellow region in the elements of drosomycin and PhD1 indicates the CSα*β* motif.

one of three disulfide bridges that are characteristic of the CSα*β* motif, the loss of the corresponding bridge indicates that DSP is not a member of the authentic CSα*β* family. This difference of disulfide bridges, especially Cys-20/Cys-41, is involved in the structural difference between DSP and PhD1. In PhD1, the α1 helix lies along with the *β*3 strand due to the presence of a pair of disulfide bridges as mentioned above, whereas the *β*-sheet and the *β*2/*β*3 loop region of DSP are distant from the longer α2 helix (Figures 2 and 3). This structural feature may agree with the fact that the resonances derived from Gly-35 and Gly-36 were not detected in the NMR spectra. In DSP, Gly-35, Gly-36, and Gly-37 are located in the *β*2/*β*3 loop region, and it is apparently expected that the loop region exhibits a higher flexibility in the DSP structure. Although similar consecutive glycine residues are also found in *γ*1-hordothionin (Gly-30, Gly-31, and Gly-32; Figure 1), their resonances can be observed and assigned together with those for residues forming the *β*2/*β*3 loop (*44*). In *γ*1-hordothionin, the consecutive glycines are located in the N-terminal segment of the *β*2 strand and show a certain degree of convergence in the solution structure. Therefore, the disappearance of NMR signals for Gly-35 and Gly-36 in DSP supports the idea that the *β*2/*β*3 loop region of DSP is highly flexible and undergoes conformational changes in solution. This effect may be due not only to the consecutive glycine residues but also to the location of the *β*2/*β*3 loop away from the longer α2 helix.

In spite of these differences, it is interesting that the overall structure of DSP resembles those of other antifungal peptides with CSα*β* motifs (Figure 3). Mutational analysis has identified the essential residues for antifungal activity of Rs-AFP, and they are largely located in the *β*1/α1 loop (corresponding to the α1 helix of DSP), at the end of the α1 helix (α2 helix of DSP), in the *β*2/*β*3 loop, and in the *β*3 strand (*25*). This region overlaps with a portion showing structural similarity with other antifungal peptides with a CSα*β* motif. Moreover, a modeling study based on the solution structure of drosomycin suggested that the hydrophobic and the proximal basic residues on the *β*-sheet contribute to the interaction of antifungal peptides with their target (*45*). DSP also has some hydrophobic residues on its *β*-sheet, such as Tyr-32 (*β*2) and Tyr-39 (*β*3), and one adjacent basic residue, Arg-3 (*β*1). Thus, the common feature of the three-dimensional structures of DSP and insect- and plant-antifungal peptides may explain the antifungal activity of DSP.

Surface Profiles of DSP and ω-Conotoxins. DSP also acts as a Ca^{2+} channel blocker in a fashion and with potency similar to those of *ω*-conotoxin GVIA (*3*). However, these two peptides do not appear to have similar overall folds, reflecting the differences in their primary amino acid sequences and their disulfide bridge patterns. Although there seems to be no structural relationship between the two peptides, we found an interesting common feature, namely, that the surface arrangement of some key residues required for the activity of *ω*-conotoxins GVIA and MVIIA is also found in the structure of DSP (Figure 4). Several groups have identified the essential residues for the channel blocking activity of GVIA and MVIIA (*15*−*17*, *46*−*48*). They have commonly reported that the replacement of Lys-2 and Tyr-13 by other amino acids in GVIA and MVIIA causes a

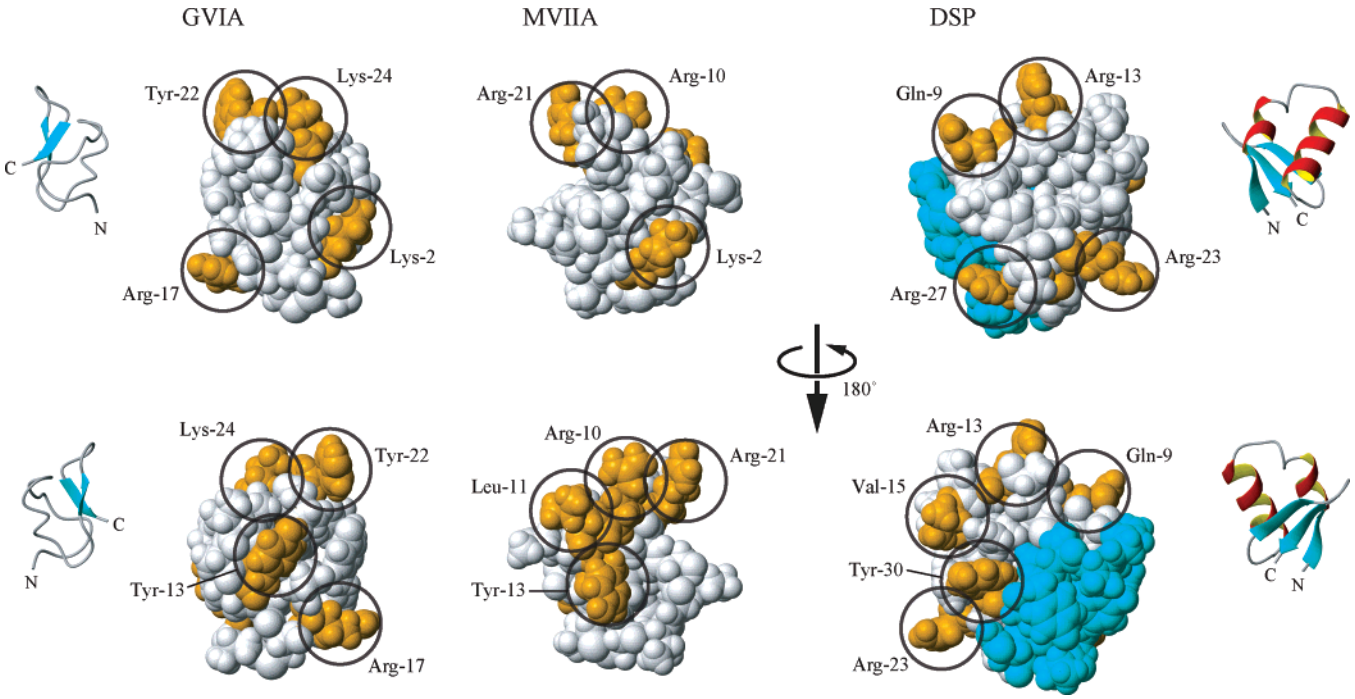

FIGURE 4: Comparison of surface residue distributions of DSP with ω-conotoxins GVIA and MVIIA. The structures of GVIA (PDB code 1OMC, left), MVIIA (1OMG, middle), and DSP (right) are depicted using a space-filling scheme. Mutational analyses of GVIA and MVIIA have revealed that the residues highlighted in orange are essential for Ca^{2+} channel-blocking activity. The DSP structure was aligned by matching the key residues with those of GVIA and MVIIA. The view in the lower panel is a 180° rotation of the upper panel around the vertical axis. The ribbon presentations of the DSP and GVIA structures are in the same orientation as the neighboring space-fill models of DSP and GVIA, respectively. The β-sheet region (residues 1−3 and 31−41) of DSP is colored cyan.

substantial loss in potency. In addition, Arg-17, Tyr-22, and Lys-24 in GVIA and Arg-10, Leu-11, and Arg-21 in MVIIA play supplemental roles in the interaction with the Ca^{2+} channel. Intriguingly, DSP has a similar distribution of surface residues: Lys-2, Tyr-13, Arg-17, and Lys-24 in GVIA correspond to Arg-23, Tyr-30, Arg-27, and Arg-13 in DSP, respectively (Figure 4). As in the case of GVIA, Lys-2, Arg-10, Leu-11, and Tyr-13 in MVIIA superimpose well on Arg-23, Arg-13, Val-15, and Tyr-30 in DSP, respectively. In GVIA, the substitution of Lys-2 by arginine has little effect on Ca^{2+} channel inhibition, whereas the potency is reduced when the positive charge is eliminated, indicating that the charge is more important than the side chain length (*17*). This concept can be applied to the comparison of GVIA and DSP; specifically, Arg-23 in DSP may behave like Lys-2 in GVIA. On the other hand, the position of Tyr-22 in GVIA overlaps with that of Gln-9 in DSP. Site-directed mutagenesis studies indicate, however, that the polarity of the hydroxyl group of the side chain of Tyr-13 and Tyr-22 contributes to the interaction between GVIA and its target (*17*). Therefore, the carbonyl group of the side chain of Gln-9 can probably mimic the hydroxyl group of Tyr-22 during the binding of DSP to Ca^{2+} channels.

In addition, the selectivity of N-type and P/Q-type Ca^{2+} channels is controlled by the second and fourth regions when the MVIIA amino acid sequence is separated by half-cystine residues (*14*). Considering that Arg-10, Leu-11, and Tyr-13 of MVIIA are located in the second region and that Arg-21 is included in the fourth, the residues highlighted in Figure 4 may also be involved in the specificity of DSP for the N-type Ca^{2+} channels.

Thus, DSP and ω-conotoxins have similar distributions of residues required for activity (Figure 4). The highlighted residues of DSP are concentrated on one face of the molecule, namely, on the surface around the α-helices, including Gln-9 in α1, Arg-13 in the α1/α2 loop, Val-15 and Arg-23 in α2, and Arg-27 in the α2/β2 loop. This feature is expected to allow DSP to interact with a Ca^{2+} channel via the α-helix region. Although DSP is larger than ω-conotoxins due to the bulk of the β-sheet, as shown in Figure 4, the β-sheet will not hinder the interaction between DSP and the Ca^{2+} channels as long as DSP binds to the target via the surface of the α-helices. Thus, it is interesting that DSP has a rational distribution of key residues, and these likely interact with the Ca^{2+} channels in a fashion similar to that in ω-conotoxins despite the lack of similarity in their three-dimensional structures. This is not surprising, because proteins with the same function may have distinct global folding patterns and/or amino acid sequences, but the local structure around the active site or the spatial geometry of the residues essential for the activity is generally conserved. Charybdotoxin, which adopts a CSαβ fold, acts as a potassium channel blocker. The interaction with the channel requires five residues (*49*, *50*). Structural studies using NMR suggested that these residues actually make contacts with the channel surface (*51*). In particular, the side chain of Lys-27 of charybdotoxin inserts into the channel pore. Intriguingly, the spatial arrangement of the functional residues including Lys-27 is conserved even in two structurally unrelated potassium channel blockers, sea anemone toxins BgK and ShK (*52*, *53*).

Our NMR data suggested that DSP has a unique structure and surface profile. Although further analyses are needed to elucidate how DSP actually achieves its functions, the solution structure of DSP provides insight into how it can act as an antifungal peptide and a Ca^{2+} channel blocker.

Recently, progress has been made in the development of peptides for clinical and agricultural use. For example, a synthetic peptide corresponding to MVIIA (also called ziconotide or SNX-111) was approved by the U.S. Food and Drug Administration for use in the management of severe chronic pain (*54*). The intriguing features of the DSP structure should help in clarifying the molecular mechanism of DSP but also in the development of useful peptides with antifungal and Ca^{2+} channel inhibitory activities.

ACKNOWLEDGMENT

We thank Dr. Tomoharu Gomi of the Life Science Research Center at the University of Toyama for helpful suggestions and discussion on the determination of half-cystine pairings.

SUPPORTING INFORMATION AVAILABLE

NOESY spectra of DSP measured at 298 K with a mixing time of 100 ms, survey of NMR data used to identify the regular secondary structure of DSP, and gel filtration chromatography analysis of DSP. This material is available free of charge via the Internet at http://pubs.acs.org.

REFERENCES

1. Tanaka, H., Sudo, C., An, Y., Yamashita, T., Sato, K., Kurihara, M., and Suzuki, K. (1998) A specific peptide produced during adult diapause of the leaf beetle, *Gastrophysa atrocyanea* Moschulsky (Coleoptara: Chrysomelidae), *Appl. Entomol. Zool. 33*, 535−543.
2. Tanaka, H., and Suzuki, K. (2005) Expression profiling of a diapause-specific peptide (DSP) of the leaf beetle *Gastrophysa atrocyanea* and silencing of DSP by double-strand RNA, *J. Insect Physiol. 51*, 701−707.
3. Tanaka, H., Sato, K., Saito, Y., Yamashita, T., Agoh, M., Okunishi, J., Tachikawa, E., and Suzuki, K. (2003) Insect diapuse-specific peptide from the leaf beetle has consensus with a putative iridovirus peptide, *Peptides 24*, 1327−1333.
4. Lomax, R. B., Michelena, P., Núñez, L., García-Sancho, J., García, A. G., and Montiel, C. (1997) Different contributions of L- and Q-type Ca^{2+} channels to Ca^{2+} signals and secretion in chromaffin cell subtypes, *Am. J. Physiol. 272*, C476−C484.
5. Pallaghy, P. K., Nielson, K. J., Craik, D. J., and Norton, R. S. (1994) A common structural motif incorporating a cystine knot and a triple-stranded β-sheet in toxic and inhibitory polypeptides, *Protein Sci. 3*, 1833−1839.
6. Narasimhan, L., Singh, J., Humblet, C., Guruprasad, K., and Blundell, T. (1994) Snail ad spider toxins share a similar tertiary structure and 'cystine motif', *Nat. Struct. Biol. 1*, 850−852.
7. Norton, R. S., and Pallaghy, P. K. (1998) The cystine knot structure of ion channel toxins and related polypeptides, *Toxicon 36*, 1573−1583.
8. Adams, M. E., Mintz, I. M., Reily, M. D., Thanabal, V., and Bean, B. P. (1993) Structure and properties of ω-agatoxin IVB, a new antagonist of P-type calcium channels, *Mol. Pharmacol. 44*, 681−688.
9. Yu, H., Rosen, M. K., Saccomano, N. A., Phillips, D., Volkmann, R. A., and Schreiber, S. L. (1993) Sequential assignment and structure determination of spider toxin ω-Aga-IVB, *Biochemistry 32*, 13123−13129.
10. Olivera, B. M., McIntosh, J. M., Cruz, L. J., Luque, F. A., and Gray, W. R. (1984) Purification and sequence of a presynaptic peptide toxin *Conus geographus* venom, *Biochemistry 26*, 2086−2090.
11. Pallaghy, P. K., Duggan, B. M., Pennington, M. W., and Norton, R. S. (1993) Three-dimensional structure in solution of the calcium channel blocker ω-conotoxin, *J. Mol. Biol. 234*, 405−420.
12. Yanagawa, Y., Abe, T., Satake, M., Odani, S., Suzuki, J., and Ishikawa, K. (1988) A novel sodium channel inhibitor from *Conus geographus*: purification, structure, and pharmacological properties, *Biochemistry 27*, 6256−6262.
13. Hill, J. M., Alewood, P. F., and Craik, D. J. (1997) Solution structure of the sodium channel antagonist conotoxin GS: a new molecular caliper for probing sodium channel geometry, *Structure 5*, 571−583.
14. Nielsen, K. J., Adams, D., Thomas, L., Bond, T. J., Alewood, P. F., Craik, D. J., and Lewis, R. J. (1999) Structure-activity relationships of ω-conotoxins MVIIA, MVIIC and 14 loop splice hybrids at N and P/Q-type calcium channels, *J. Mol. Biol. 289*, 1405−1421.
15. Kim, J. I., Takahashi, M., Ogura, A., Kohno, T., Kudo, Y., and Sato, K. (1994) Hydroxyl group of Tyr^{13} is essential for the activity of ω-conotoxin GVIA, a peptide toxin for N-type calcium channel, *J. Biol. Chem. 269*, 23876−23878.
16. Lew, M. J., Flinn, J. P., Pallaghy, P. K., Murphy, R., Whorlow, S. L., Wright, C. E., Norton, R. S., and Angus, J. A. (1997) Structure-function relationships of ω-conotoxin GVIA, *J. Biol. Chem. 272*, 12014−12023.
17. Flinn, J. P., Pallaghy, P. K., Lew, M. J., Murphy, R., Angus, J. A., and Norton, R. S. (1999) Roles of key functional groups in ω-conotoxin GVIA, *Eur. J. Biochem. 262*, 447−455.
18. Cornet, B., Bonmatin, J.-M., Hetru, C., Hoffmann, J. A., Ptak, M., and Vovelle, F. (1995) Refined three-dimensional solution structure of insect defensin A, *Structure 3*, 435−448.
19. Landon, C., Sodano, P., Hetru, C., Hoffmann, J., and Ptak, M. (1997) Solution structure of drosomycin, the first inducible antifungal protein from insects, *Protein Sci. 6*, 1878−1884.
20. Fant, F., Vranken, W., Broekaert, W., and Borremans, F. (1998) Determination of the three-dimensional solution structure of *Raphanus sativus* antifungal protein by ^{1}H NMR, *J. Mol. Biol. 279*, 257−270.
21. Fehlbaum, P., Bulet, P., Michaut, L., Lagueux, M., Broekaert, W. F., Hetru, C., and Hoffmann, J. A. (1994) Insect Immunity. Septic injury of Drosophila induces the synthesis of a potent antifungal peptide with sequence homology to plant antifungal peptides, *J. Biol. Chem. 269*, 33159−33163.
22. Terras, F. R. G., Schoofs, H. M. E., De Bolle, M. F. C., Van Leuven, F., Rees, S. B., Vanderleyden, J., Cammue, B. P. A., and Broekaert, W. F. (1992) Analysis of two novel classes of plant antifungal proteins from radish (*Raphanus sativus* L.) seeds, *J. Biol. Chem. 267*, 15301−15309.
23. Spelbrink, R. G., Dilmac, N., Allen, A., Smith, T. J., Shah, D. M., and Hockerman, G. H. (2004) Differential antifungal and calcium channel-blocking activity among structurally related plant defensins, *Plant Physiol. 135*, 2055−2067.
24. Thevissen, K., Ghazi, A., De, Samblanx, G. W., Brownlee, C., Osborn, R. W., and Broekaert, W. F. (1996) Fungal membrane responses induced by plant defensins and thionins, *J. Biol. Chem. 271*, 15018−15025.
25. De Samblanx, G. W., Goderis, I. J., Thevissen, K., Raemaekers, R., Fant, F., Borremans, F., Acland, D. P., Osborn, R. W., Patel, S., and Broekaert, W. F. (1997) Mutational analysis of a plant defensin from radish (*Raphanus sativus* L.) reveals two adjacent sites important for antifungal activity, *J. Biol. Chem. 272*, 1171−1179.
26. Thevissen, K., Warnecke, D. C., Francois, I. E., Leipelt, M., Heinz, E., Ott, C., Zahringer, U., Thomma, B. P., Ferket, K. K., and Cammue, B. P. (2004) Defensins from insects and plants interact with fungal glucosylceramides, *J. Biol. Chem. 279*, 3900−3905.
27. Pace, C. N., Vajdos, F., Fee, L., Grimsley, G., and Gray, T. (1995) How to measure and predict the molar absorption coefficient of a protein, *Protein Sci. 4*, 2411−2423.
28. Rance, M., Sørensen, O. W., Bodenhausen, G., Wagner, G., Ernst, R. R., and Wüthrich, K. (1983) Improved spectral resolution in COSY ^{1}H NMR spectra of proteins via double quantum filtering, *Biochem. Biophys. Res. Commun. 117*, 479−485.
29. Braunschweiler, L., and Ernst, R. R. (1983) Coherence transfer by isotropic mixing: application to proton correlation spectroscopy, *J. Magn. Reson. 53*, 521−528.
30. Kumar, A., Ernst, R. R., and Wüthrich, K. (1980) A two-dimensional nuclear Overhauser enhancement (2D NOE) experiment for the elucidation of complete proton-proton cross-relaxation networks in biological macromolecules, *Biochem. Biophys. Res. Commun. 9*, 1−6.
31. Sklenar, V., Piotto, M., Leppik, R., and Saudek, V. (1993) Gradient-tailored water suppression for ^{1}H-^{15}N HSQC experiments optimized to retain full sensitivity, *J. Magn. Reson., Ser. A 102*, 241−245.
32. Wüthrich, K. (1986) *NMR of Proteins and Nucleic Acid*, John Wiley & Sons Inc., New York.
33. Delaglio, F., Grzesiek, S., Vuister, G. W., Zhu, G., Pfeifer, J., and Bax, A. (1995) NMRPipe: A multidimensional spectral processing system based on UNIX pipes, *J. Biomol. NMR 6*, 277−293.

34. Garrett, D. S., Powers, R., Gronenborn, A. M., and Clore, G. M. (1991) A common sense approach to peak picking two-, three- and four-dimensional spectra using automatic computer analysis of contour diagrams, *J. Magn. Reson. 95*, 214−220.
35. Johnson, B. A., and Blevins, R. A. (1994) NMRView: A computer program for the visualization and analysis of NMR data, *J. Biomol. NMR 4*, 603−614.
36. Güntert, P., Mumenthaler, C., and Wüthrich, K. (1997) Torsion angle dynamics for NMR structure calculation with the new program DYANA, *J. Mol. Biol. 273*, 283−298.
37. Herrmann, T., Güntert, P., and Wüthrich, K. (2002) Protein NMR structure determination with automated NOE assignment using the new software CANDID and the torsion angle dynamics algorithm DYANA, *J. Mol. Biol. 319*, 209−227.
38. Brünger, A. T. (1992) *X-PLOR version 3.1*, Yale University Press, New Haven, CT.
39. Koradi, R., Billeter, M., and Wüthrich, K. (1996) MOLMOL: a program for display and analysis of macromolecular structures, *J. Mol. Graphics 14*, 51−55.
40. Laskowski, R. A., Rullman, J. A., MacArthur, M. W., Kaptein, R., and Thornton, J. M. (1996) AQUA and PROCHECK-NMR: programs for checking the quality of protein structures solved by NMR, *J. Biomol. NMR 8*, 477−486.
41. Holm, L., and Sander, C. (1993) Protein structure comparison by alignment of distance matrices, *J. Mol. Biol. 233*, 123−138.
42. Akiyama, Y., Onizuka, K., Noguchi, T., and Ando, M. (1998) Parallel protein information analysis (PAPIA) system running on a 64-node PC cluster, *Genome Inform. Ser. Workshop Genome Inform. 9*, 131−140.
43. Janssen, B. J., Schirra, H. J., Lay, F. T., Anderson, M. A., and Craik, D. J. (2003) Structure of Petunia hybrida defensin 1, a novel plant defensin with five disulfide bonds, *Biochemistry 42*, 8214−8222.
44. Bruix, M., Jiménez, M. A., Santoro, J., González, C., Colilla, F. J., Méndez, E., and Rico, M. (1993) Solution structure of γ1-H and γ1-P thionins from barley and wheat endosperm determined by ^{1}H NMR: a structural motif common to toxic arthropod proteins, *Biochemistry 32*, 715−724.
45. Landon, C., Pajon, A., Vovelle, F., and Sodano, P. (2000) The active site of drosomycin, a small insect antifungal protein, delineated by comparison with the modeled structure of Rs-AFP2, a plant antifungal protein, *J. Peptide Res. 56*, 231−238.
46. Kim, J. I., Takahashi, M., Ohtake, A., Wakamiya, A., and Sato, K. (1995) Tyr^{13} is essential for the activity of ω-conotoxin MVIIA and GVIA, specific N-type calcium channel blockers, *Biochem. Biophys. Res. Commun. 206*, 449−454.
47. Nadasdi, L., Yamashiro, D., Chung, D., Tarczy-Hornoch, K., Adriaenssens, P., and Ramachandran, J. (1995) Structure-activity analysis of a *Conus* peptide blocker of N-type neuronal calcium channels, *Biochemistry 34*, 8076−8081.
48. Wang, Y. X., Bezprozvannaya, S., Bowersox, S. S., Nadasdi, L., Miljanich, G., Mezo, G., Silva, D., Tarczy-Hornoch, K., and Luther, R. R. (1998) Peripheral versus central potencies of N-type voltage-sensitive calcium channel blockers, *Arch. Pharmacol. 357*, 159−168.
49. Bontems, F., Gilquin, B., Roumestand, C., Ménez, A., and Toma, F. (1992) Analysis of side-chain organization on a refined model of charybdotoxin: structural and functional implications, *Biochemistry 31*, 7756−7764.
50. Goldstein, S. A. N., Pheasant, D. J., and Miller, C. (1994) The charybdotoxin receptor of a shaker K^+ channel: peptide and channel residues mediating molecular recognition, *Neuron 12*, 1377−1388.
51. Yu, L., Sun, C., Song, D., Shen, J., Xu, N., Gunasekera, A., Hajduk, P. J., and Olejniczak, E. T. (2005) Nuclear magnetic resonance structural studies of a potassium channel-charybdotoxin complex, *Biochemistry 44*, 15834−15841.
52. Dauplais, M., Lecoq, A., Song, J., Cotton, J., Jamin, N., Gilquin, B., Roumestand, C., Vita, C., de Medeiros, C. L. C., Rowan, E. G., Harvey, A. L., and Ménez, A. (1997) On the convergent evolution of animal toxins: conservation of a diad of functional residues in potassium channel-blocking toxins with unrelated structures, *J. Biol. Chem. 272*, 4302−4309.
53. Norton, R. S., Pennington, M. W., and Wulff, H. (2004) Potassium channel blockade by the sea anemone toxin ShK for the treatment of multiple sclerosis and other autoimmune diseases, *Curr. Med. Chem. 11*, 3041−3052.
54. McGivern, J. P. (2006) Targeting N-type and T-type calcium channels for the treatment of pain, *Drug Discovery Today 11*, 245−253.

BI701319T